Testing models for anomalous radiative decays of the Z boson

V. Barger, H. Baer, and K. Hagiwara
Physics Department, University of Wisconsin, Madison, Wisconsin 53706
(Received 8 May 1984)

The following models for radiative decays of the Z boson into a lepton pair and a photon are studied, with cuts appropriate to the CERN $p\bar{p}$ collider experiments: (i) bremsstrahlung in the standard model, (ii) a pseudoscalar partner of Z, (iii) excited leptons, (iv) an anomalous $ZZ\gamma$ coupling, and (v) an anomalous $Z\gamma\gamma$ coupling. Dalitz plots for the $l^+l^-\gamma$ final state are shown to be particularly well suited to distinguish and test the models; none of the alternative models provides a likely explanation of the observed events.

I. INTRODUCTION

The observation at the CERN $p\bar{p}$ collider of the W and Z bosons[1,2] at their predicted masses seemed to confirm the standard electroweak theory.[3] However, two of eight candidates for Z decay to e^+e^- contain a hard photon,[2,4] which is considerably more than expected from bremsstrahlung.[5] To explain this seemingly copious radiative Z decay, a number of alternative models have been proposed.[6–10] These include a hyperfine partner of the Z boson,[6] an excited electron,[7] an anomalous $ZZ\gamma$ coupling,[8] an anomalous $Z\gamma\gamma$ coupling,[9] and a current[10] which couples to $Z\gamma$. In this paper we contrast the predicted distributions of these models and show that Dalitz plots for the $l^+l^-\gamma$ final state are particularly well suited to distinguish and test the models. In the following we first briefly introduce each of the above models; then we examine their Dalitz plots, l^+l^- and $l\gamma$ invariant-mass distributions, and γ transverse-momentum distributions. We conclude that none of the models provides a likely explanation of the observed events.

In model calculations we take $M_Z=94$ GeV, $\Gamma_Z=3$ GeV, $\sin^2\theta_W=0.22$, and $\alpha=1/128$ and use the parton distributions of Duke and Owens.[11] The squared matrix elements of the $q\bar{q}\to l^+l^-\gamma$ subprocesses are evaluated using ASHMEDAI and checked by hand. Unless otherwise stated, the following cuts are imposed in accordance with typical experimental acceptance conditions:

$$\max(p_{lT})>15\text{ GeV},\quad p_{\gamma T}>15\text{ GeV}\,,$$

$$\theta(i,\text{beam})>5^\circ,\quad \theta(i,j)>5^\circ\,,$$

and

$$|\,m(l^+l^-\gamma)-m_Z\,|<10\text{ GeV}\,.$$

Here p_T denotes momentum transverse to the beam and i,j denote l^+, l^-, or γ.

The details of the various models are given in Sec. II and the comparisons with experiment are made in Sec. III.

II. MODELS

A. Standard model

The differential cross section for $e^+e^-\to q\bar{q}\gamma$ is given by Berends, Kleiss, and Jadach.[12] By crossing we obtain the parton-subprocess cross section for $q\bar{q}\to e^+e^-\gamma$. Since our final-state cuts avoid mass singularities, we can safely neglect quark and lepton masses. With our cuts we find

$$\sigma(p\bar{p}\to e^+e^-\gamma)/\sigma(p\bar{p}\to Z\to e^+e^-)=2\%\,.$$

This roughly agrees with the estimate (1.6%) obtained by using the Sterman-Weinberg formula[13] for unpolarized $Z\to e^+e^-\gamma$ decay:

$$\frac{\Gamma(Z\to e^+e^-\gamma;E_\gamma>m_Z\epsilon,\theta_{ij}>2\delta)}{\Gamma(Z\to e^+e^-X)}=\frac{\alpha}{\pi}\left[(4\ln 2\epsilon+3)\ln\delta+\frac{\pi^2}{3}-\frac{7}{4}+O(\delta,\epsilon)\right] \tag{2.1}$$

with $\epsilon=15\text{ GeV}/m_Z$ and $2\delta=5^\circ$ as the minimum angular separation of any two final-state particles.

B. Scalar partner of Z (Ref. 6)

In this model Z decays radiatively into a pseudoscalar (or scalar) partner U plus a photon; U decays into l^+l^- with a universal Yukawa coupling to all lepton and quark flavors. The interaction Lagrangian of a pseudoscalar U_P and a scalar U_S reads

$$\mathscr{L}=U_P\left[\frac{f_P}{\Lambda}\tilde{F}_{\mu\nu}(\partial^\mu Z^\nu)+\sum_f ig_P^{Uff}\bar{\psi}_f\gamma_5\psi_f\right]+U_S\left[\frac{f_S}{\Lambda}F_{\mu\nu}(\partial^\mu Z^\nu)+\sum_f g_S^{Uff}\bar{\psi}_f\psi_f\right], \tag{2.2}$$

where $F_{\mu\nu}=\partial_\mu A_\nu-\partial_\nu A_\mu$, $\tilde{F}_{\mu\nu}=\frac{1}{2}\epsilon_{\mu\nu\rho\sigma}F^{\rho\sigma}$, and a mass scale Λ has been introduced to make the couplings f_P and f_S dimensionless. With the ansatz of a universal Yukawa coupling, $g_P^{Uff}=g_P$ or $g_S^{Uff}=g_S$ for any fermion. In momentum space the gauge-invariant $ZU\gamma$ vertices are

$$\Gamma^{\mu\nu}(P,p,k)=i\frac{f_P}{\Lambda}\epsilon^{\mu\nu\lambda\sigma}P_\lambda k_\sigma+i\frac{f_S}{\Lambda}[k^\mu P^\nu-(k\cdot P)g^{\mu\nu}]\,, \tag{2.3}$$

where μ and ν denote Z and γ polarization indices, and P, p, and k are the four momenta of Z, U, and γ, respectively. The amplitude for the subprocess $q\bar{q}\to Z\to U_P\gamma$, $U_P\to l\bar{l}$ is

$$\mathcal{M}=\frac{ef_P g_P}{\Lambda}D_Z(P^2)D_U(p^2)\epsilon^{\mu\nu\lambda\sigma}P_\lambda k_\sigma \times\bar{v}(\bar{q})\gamma_\mu(g_V^q-g_A^q\gamma_5)u(q)\bar{u}(l)\gamma_5 v(\bar{l})\epsilon_\nu^*(k)\ , \tag{2.4}$$

where q, $\bar{q}$, l, and $\bar{l}$ denote particle momenta and

$$D_B(t)=\frac{1}{t-m_B{}^2+im_B\Gamma_B} \tag{2.5}$$

denotes the boson propagator factor; the Z-boson—fermion couplings are defined by the interaction Lagrangian

$$\mathcal{L}=\sum_f e\bar{\psi}_f\gamma_\mu(g_V^f-g_A^f\gamma_5)\psi_f Z^\mu\ . \tag{2.6}$$

The spin- and color-summed matrix element squared is

$$\sum|\mathcal{M}|^2=\frac{2Ce^2f_P{}^2g_P{}^2}{\Lambda^2}[(g_V^q)^2+(g_A^q)^2]\,|D_Z(P^2)|^2\,|D_U(p^2)|^2P^2p^2[(P^2-p^2)^2-8(q\cdot k)(\bar{q}\cdot k)] \tag{2.7}$$

with the color factor $C=3$. The subprocess cross section reads

$$d\hat{\sigma}=\frac{1}{8C^2\hat{s}}\sum|\mathcal{M}|^2(2\pi)^4\delta^4(P-l-\bar{l}-k) \times\prod_{i=l,\bar{l},k}\frac{d^3p_i}{(2\pi)^3 2E_i} \tag{2.8}$$

with $\hat{s}=P^2$. In fact, the scalar-U case gives an identical result,[14] with the subscript P replaced by S in Eq. (2.7). If both pseudoscalar and scalar U bosons exist, their contributions add incoherently. Subsequently we illustrate the case of a single U boson with mass $m_U=50$ GeV and an effective width $\Gamma_U=2$ GeV which represents the combined effects of the U width and the experimental resolution.

C. Excited electron (Ref. 7)

Here the $ee\gamma$ events are presumed to originate from $Z\to e^*\bar{e},e\bar{e}^*$ transitions with subsequent $e^*\to e\gamma$ decay. We assume that the e^* has spin $\frac{1}{2}$ and forms a weak doublet

$$L^*=\begin{bmatrix}\nu^*\\ e^*\end{bmatrix}$$

with an excited neutrino ν^*. The transition couplings between L^* and the electron doublet

$$l_L=\begin{bmatrix}\nu_e\\ e\end{bmatrix}_L$$

are specified by the interaction Lagrangian

$$\mathcal{L}=\frac{gf}{\Lambda}\left[\bar{L}^*\sigma_{\mu\nu}\frac{\vec{\tau}}{2}l_L\right]\partial^\mu\vec{W}^\nu +\frac{g'f'}{\Lambda}(\bar{L}^*\sigma_{\mu\nu}Yl_L)\partial^\mu B^\nu+\text{H.c.}\ , \tag{2.9}$$

where g and g' are the standard model SU(2) and U(1) coupling constants, f and f' are the dimensionless transition magnetic moments, $\vec{\tau}$ denotes the Pauli matrices, $Y=-\frac{1}{2}$ is the U(1) charge, and

$$\sigma_{\mu\nu}=\frac{i}{2}(\gamma_\mu\gamma_\nu-\gamma_\nu\gamma_\mu)\ .$$

In momentum space the Vf^*f_L vertices are

$$\Gamma^\mu=-\sigma^{\mu\nu}q_\nu\frac{G_V}{\Lambda}\ , \tag{2.10}$$

where q is the momentum transfer and

$$G_Z=e(I_3f\cot\theta_W-Yf'\tan\theta_W)\ , \tag{2.11}$$

$$G_\gamma=e(I_3f+Yf')\ . \tag{2.12}$$

Note that $G_\gamma=0$ for $\nu\nu^*$ when $f=f'$, and $G_\gamma=0$ for ee^* when $f+f'=0$.

The amplitude for $q\bar{q}\to l^*l$ or $l\bar{l}^*$, $l^*\to l\gamma$ is

$$\mathcal{M}=\frac{ieG_ZG_\gamma}{\Lambda^2}D_Z(P^2)[\bar{v}(\bar{q})\gamma_\nu(g_V^q-g_A^q\gamma_5)u(q)]\left[\bar{u}(l)\frac{1+\gamma_5}{2}\left[\frac{\not{\epsilon}\not{k}(\not{k}+\not{l}+M)\gamma^\nu\not{P}}{(l+k)^2-M^2+iM\Gamma}-\frac{\gamma^\nu\not{P}(\not{k}+\not{\bar{l}}-M)\not{\epsilon}\not{k}}{(\bar{l}+k)^2-M^2+iM\Gamma}\right]\frac{1-\gamma_5}{2}v(\bar{l})\right]\ , \tag{2.13}$$

where ϵ is the photon polarization vector, $M=m_{e^*}$ and $\Gamma=\Gamma_{e^*}$. The expression for the spin- and color-summed matrix element squared is rather lengthy and will not be shown here. We remark that the dependence on the transition form factors f and f' factorizes in the amplitude (2.13) and thus the shape of the distributions does not depend on a particular choice of their values insofar as G_ZG_γ is nonvanishing. In our illustration we choose $m_{e^*}=80$ GeV, and $\Gamma_{e^*}=2$ GeV, where Γ represents both true width and experimental resolution.

D. Anomalous $ZZ\gamma$ coupling (Ref. 8)

In a composite model for weak bosons, Gounaris, Kögerler, and Schildknecht proposed a strong $ZZ\gamma$ coupling. For on-shell γ, there are two independent gauge-invariant dimension-six interaction terms

$$\mathscr{L}=\frac{f_1}{\Lambda^2}\tilde{F}_{\mu\nu}Z^\mu\partial^\lambda\partial_\lambda Z^\nu+\frac{f_2}{\Lambda^2}F_{\mu\nu}Z^\mu\partial^\lambda\partial_\lambda Z^\nu \ . \tag{2.14}$$

Here a possible coupling of the spin-0 part of Z^μ (i.e., $\partial_\mu Z^\mu$) is neglected.[15] The $Z^\mu(P)$-$Z^\nu(p)$-$A^\rho(k)$ vertex in the momentum space reads

$$\Gamma^{\mu\nu\rho}(P,p,k)=\frac{P^2-p^2}{\Lambda^2}[f_1\epsilon^{\alpha\mu\nu\rho}k_\alpha+f_2(k^\mu g^{\nu\rho}-k^\nu g^{\mu\rho})] \ , \tag{2.15}$$

which manifestly exhibits electromagnetic gauge invariant and Bose statistics for the two Z bosons. In the following we set the CP-odd coupling f_2 to zero.

The amplitude for $q\bar{q}\to Z\to Z\gamma$, $Z\to l\bar{l}$ via the anomalous $ZZ\gamma$ coupling reads

$$\mathscr{M}=e^2D_Z(P^2)D_Z(p^2)\Gamma^{\mu\nu\rho}\bar{v}(\bar{q})\gamma_\mu(g_V^q-g_A^q\gamma_5)u(q)\bar{u}(l)\gamma_\nu(g_V^l-g_A^l\gamma_5)v(\bar{l})\epsilon_\rho^*(k) \ . \tag{2.16}$$

The spin- and color-summed matrix element squared is given by

$$\begin{aligned}\sum|\mathscr{M}|^2=&2^5e^4Cf_1{}^2\frac{(\hat{s}-p^2)^2}{\Lambda^4}|D_Z(\hat{s})|^2|D_Z(p^2)|^2\\ &\times\{[(g_V^q)^2+(g_A^q)^2][(g_V^l)^2+(g_A^l)^2][k\cdot q(\bar{q}\cdot l\,k\cdot\bar{l}+\bar{q}\cdot\bar{l}\,k\cdot l)+k\cdot\bar{q}(q\cdot l\,k\cdot\bar{l}+q\cdot\bar{l}\,k\cdot l)]\\ &+4g_V^qg_A^qg_V^lg_A^l[k\cdot q(\bar{q}\cdot l\,k\cdot\bar{l}-\bar{q}\cdot\bar{l}\,k\cdot l)-k\cdot\bar{q}(q\cdot l\,k\cdot\bar{l}-q\cdot\bar{l}\,k\cdot l)]\} \ .\end{aligned} \tag{2.17}$$

After integrating over the $l\bar{l}$ phase space, disregarding any experimental cuts, the following compact expression for the differential cross section is obtained:

$$\frac{d\hat{\sigma}}{dx\,d\cos\hat{\theta}_\gamma}=\frac{\alpha^2f_1{}^2[(g_V^q)^2+(g_A^q)^2][(g_V^l)^2+(g_A^l)^2]}{192\pi C\Lambda^4}|D_Z(\hat{s})D_Z(p^2)|^2\hat{s}^5(1-x)^5[1+2x+(1-2x)\cos^2\hat{\theta}_\gamma] \ . \tag{2.18}$$

Here $\hat{s}=P^2$, $x=m_{l\bar{l}}{}^2/\hat{s}$, and $\hat{\theta}_\gamma$ denotes the opening angle between the γ and quark momentum in the $q\bar{q}$ c.m. frame. Although we perform all the numerical calculations by using the exact matrix element squared and the experimental cuts, the formula (2.18) turns out to be useful in understanding the qualitative behavior of the $m_{l\bar{l}}$ and $p_{\gamma T}$ distributions.

E. Anomalous $Z\gamma\gamma$ coupling (Ref. 9)

In this model a strong $Z\gamma\gamma$ coupling is postulated. There are two gauge-invariant dimension-six interactions[9]

$$\mathscr{L}=\frac{1}{\Lambda^2}Z_\mu[g_1(\partial^\rho\tilde{F}^{\mu\nu})F_{\nu\rho}+g_2\tilde{F}^{\mu\nu}(\partial^\rho F_{\nu\rho})] \ , \tag{2.19}$$

which lead to the following $Z^\mu(P)-A^\nu(p)-A^\rho(k)$ vertices in the momentum space

$$\begin{aligned}\Gamma^{\mu\nu\rho}(P,p,k)=&\frac{g_1}{\Lambda^2}\{\epsilon_{\alpha\beta}{}^{\mu\rho}k^\alpha[p^\beta k^\nu-(p\cdot k)g^{\beta\nu}]+\epsilon_{\alpha\beta}{}^{\mu\nu}p^\alpha[k^\beta p^\rho-(k\cdot p)g^{\beta\rho}]\}\\ &+\frac{g_2}{\Lambda^2}\{\epsilon_{\alpha\beta}{}^{\mu\rho}k^\alpha[p^\beta p^\nu-p^2g^{\beta\nu}]+\epsilon_{\alpha\beta}{}^{\mu\nu}p^\alpha[k^\beta k^\rho-k^2g^{\beta\rho}]\} \ .\end{aligned} \tag{2.20}$$

The amplitude for $q\bar{q}\to Z\to\gamma\gamma^*$, $\gamma^*\to l\bar{l}$ is

$$\mathscr{M}=-e^2D_Z(P^2)D_\gamma(p^2)\Gamma^{\mu\nu\rho}\bar{v}(\bar{q})\gamma_\mu[g_V^q-g_A^q\gamma_5]u(q)\bar{u}(l)\gamma_\nu v(\bar{l})\epsilon_\rho^*(k) \ . \tag{2.21}$$

For the simplified case $g_1=0$ the matrix element squared with spin and color summation is

$$\sum|\mathscr{M}|^2=\frac{2^5g_2{}^2e^4C}{\Lambda^4}[(g_V^q)^2+(g_A^q)^2]|D_Z(\hat{s})|^2[k\cdot q(\bar{q}\cdot l\,k\cdot\bar{l}+\bar{q}\cdot\bar{l}\,k\cdot l)+k\cdot\bar{q}(q\cdot l\,k\cdot\bar{l}+q\cdot\bar{l}\,k\cdot l)] \ . \tag{2.22}$$

Integrating over the $l\bar{l}$ phase space ignoring the final-state cuts, the following compact expression for the differential cross section is obtained for arbitrary g_1 and g_2:

$$\frac{d\hat{\sigma}}{dx\,d\cos\hat{\theta}_\gamma}=\frac{\alpha^2[(g_V^q)^2+(g_A^q)^2]}{96\pi C\Lambda^4}|D_Z(\hat{s})|^2\hat{s}^3(1-x)^3[g_1{}^2+g_2{}^2-\tfrac{1}{2}(g_1-g_2)^2(1-2x)\sin^2\hat{\theta}_\gamma] \ . \tag{2.23}$$

Because of Yang's theorem,[16] which forbids $Z\to\gamma\gamma$ decay, there is no propagator factor $(1/p^2)^2$ left in the $Z\to e^+e^-\gamma$ decay rate to enhance small e^+e^- invariant masses. Actually, we find distributions of the anomalous $Z\gamma\gamma$ coupling model with acceptance cuts to be quite similar to the distributions from the $ZZ\gamma$ model. This can be qualitatively understood by comparing the expressions in Eqs. (2.18) and (2.23). The distributions of the $Z\gamma\gamma$ model shown later are for the special case $g_1=0$.

F. A new vector boson

It is also possible that the lepton pairs couple to a new vector boson J. Following Duncan and Veltman,[10] we assume that J couples to fermions via conventional currents, i.e., a linear combination of the weak isospin and hypercharge neutral currents. The Jff couplings can then be expressed as

$$\mathscr{L}=\sum_f e\bar{\psi}_f\gamma_\mu(G_V^f-G_A^f\gamma_5)\psi_f J^\mu \ , \tag{2.24}$$

where

$$G_V^f=\left[\frac{a-b}{2}\right]I_3+be_f \ , \qquad G_A^f=\left[\frac{a-b}{2}\right]I_3 \ , \tag{2.25}$$

with arbitrary a and b; in the standard model, $a=-1/b=\cot\theta_W$ for the Z-boson coupling and $a=b=1$ for the γ coupling. Predictions for e^+e^- distributions depend crucially on the Lorentz structure of the $ZJ\gamma$ vertex and on the mass m_J of the boson associated with the current. Unlike the $ZZ\gamma$ and $Z\gamma\gamma$ couplings of the preceding models, it is not possible to have a dimension-four interaction of the form

$$\mathscr{L}=h_1\tilde{F}_{\mu\nu}J^\mu Z^\nu+h_2F_{\mu\nu}J^\mu Z^\nu \tag{2.26}$$

which leads to the $Z^\mu(P)$-$J^\nu(p)$-$A^\rho(k)$ vertex

$$\Gamma^{\mu\nu\rho}(P,p,k)=h_1\epsilon^{\alpha\mu\nu\rho}k_\alpha+h_2(k^\mu g^{\nu\rho}-k^\nu g^{\mu\rho}) \ . \tag{2.27}$$

One of the two couplings is CP-odd; which one depends on the CP property of the J boson. By comparing Eq. (2.27) with the $ZZ\gamma$ coupling (2.15), we find that the production cross section for the subprocess $q\bar{q}\to Z\to J\gamma$; $J\to l\bar{l}$ can be obtained from the corresponding one via the $ZZ\gamma$ coupling by the following replacements:

$$\frac{P^2-p^2}{\Lambda^2}f_i\to h_i \quad (i=1,2) \ , \qquad D_Z(p^2)\to D_J(p^2) \ , \qquad (g_V^l,g_A^l)\to(G_V^l,G_A^l) \ . \tag{2.28}$$

We remark that the cross section with $h_1=0$, $h_2=h$ is identical to the cross section with $h_1=h$, $h_2=0$. For example, the partially integrated cross section over the $l\bar{l}$ phase space can be obtained from Eq. (2.18):

$$\frac{d\hat{\sigma}}{dx\,d\cos\hat{\theta}_\gamma}=\frac{\alpha^2h^2[(g_V^q)^2+(g_A^q)^2][(G_V^l)^2+(G_A^l)^2]}{192\pi C}|D_Z(\hat{s})D_J(p^2)|^2\hat{s}^3(1-x)^3[1+2x+(1-2x)\cos^2\hat{\theta}_\gamma] \ , \tag{2.29}$$

where the identity $P^2-p^2=\hat{s}(1-x)$ has been used. The resulting $e^+e^-\gamma$ distributions are similar to those of the $ZU\gamma$ model when $M_J\sim m_U\sim 50$ GeV and to the $ZZ\gamma$ model when $M_J\gg M_Z$. If $M_J\simeq M_Z$, the gross features of the distributions are still similar to the $ZZ\gamma$ model, while higher $x=m_{l\bar{l}}^2/\hat{s}$ values are more favored. We do not show distributions for the $ZJ\gamma$ model because of this ambiguity.

III. RESULTS

A. Dalitz plots

Figure 1 illustrates the Dalitz plots of the $l^+l^-\gamma$ expected in the standard model along with the corresponding three data points. The horizontal, vertical, and diagonal axes measure, respectively,

$$x_L=[\text{lower } m(l\gamma)^2]/m(l^+l^-\gamma)^2 \ , \quad x_H=[\text{higher } m(l\gamma)^2]/m(l^+l^-\gamma)^2 \ , \quad x=m(l^+l^-)^2/m(l^+l^-\gamma)^2 \ . \tag{3.1}$$

These satisfy the relation

$$x_L+x_H+x=1 \ . \tag{3.2}$$

The two published events[2] are plotted as a solid circle (UA1 event) and a solid square (UA2 event). An unpublished $\mu\bar{\mu}\gamma$ event[4] is also plotted as a triangle. In Fig. 2, we show corresponding predictions of (a) the scalar-U model, (b) the excited-lepton model, and (c) the $ZZ\gamma$ or $Z\gamma\gamma$ model. The Dalitz plots of the $ZZ\gamma$ model and the $Z\gamma\gamma$ model are virtually indistinguishable.

Of the above models only the standard model predicts

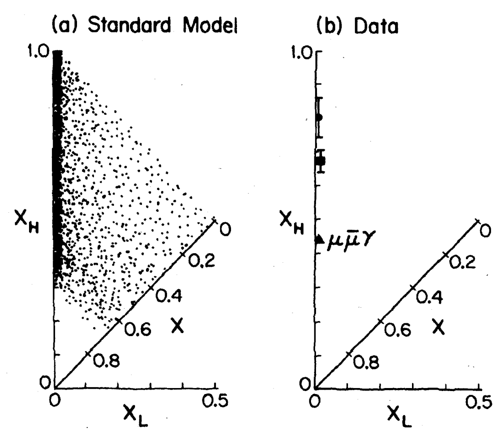

FIG. 1. (a) Dalitz plot for the process $p\bar{p}\to l^+l^-\gamma$ + anything, in the standard model with cuts as described in the text. (b) Dalitz-plot locations of data points from Refs. 2 ($e^+e^-\gamma$) and 4 ($\mu^+\mu^-\gamma$).

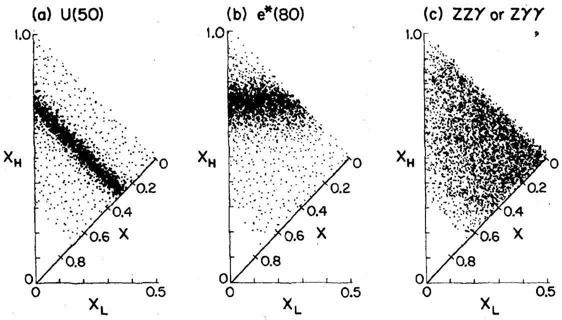

FIG. 2. Dalitz plots for the process $p\bar{p}\to l^+l^-\gamma$ + anything, for alternative models of radiative Z decay with cuts. The models illustrated are (a) $Z\to U\gamma$ with $m_U=50$ GeV, (b) $Z\to e^*\bar{e}+e\bar{e}^*$ with $m_{e^*}=80$ GeV, and (c) $Z\to Z^*\gamma$ or $\gamma^*\gamma$.

the absolute $e^+e^-\gamma$ event rate. With acceptance cuts described previously, we find

$$\sigma(p\bar{p}\to Z\to e^+e^-\gamma)/\sigma(p\bar{p}\to Z\to e^+e^-)=0.02 \quad (3.3)$$

which is much less than the observed rate of $\sim\frac{1}{3}$. It is interesting to note, however, that data points occur in the small x_L region where bremsstrahlung probabilities are highest: see Fig. 1(a).

The U signal is a band at $x=m_U{}^2/m_Z{}^2$ and the e^* signal is a band at $x_H=m_{e^*}{}^2/m_Z{}^2$, as shown in Figs. 2(a) and 2(b), respectively. In the $ZZ\gamma$ model or the $Z\gamma\gamma$ model no band structure is present in the Dalitz plot, provided that the cut $|m(l^+l^-\gamma)-m_Z|<10$ GeV is imposed; otherwise the $m(l^+l^-)$ distribution in the $ZZ\gamma$ model peaks close to m_Z while the $Z\gamma\gamma$ predictions are insensitive to the cut. This sensitivity of the $ZZ\gamma$ model prediction on the cut is a consequence of the high-energy behavior of the $q\bar{q}\to Z\gamma$ subprocess cross section in this model, discussed below.

In all of the alternative models the probability for events to occur at small x_L is low. However, the most striking feature of the observed $e^+e^-\gamma$ events is the smallness of the x_L values. The unpublished $\mu^+\mu^-\gamma$ event also has a low x_L value.

B. Invariant-mass distributions

Figure 3(a) shows the $m(l^+l^-\gamma)=(\hat{s})^{1/2}$ distribution for the various models. The $(\hat{s})^{1/2}$ distributions are shown without the $|(\hat{s})^{1/2}-m_Z|<10$ GeV cut. The low-mass tail in the standard model (SM) is due to the virtual-photon intermediate state. Most $l^+l^-\gamma$ events survive the $|(\hat{s})^{1/2}-m_Z|$ cut in all the models but the $ZZ\gamma$ model. The high-$m(l^+l^-\gamma)$ bump in the $ZZ\gamma$ model is due to its very large $q\bar{q}\to Z\gamma$ production cross section at high $(\hat{s})^{1/2}$.

The asymptotic $(\hat{s})^{1/2}$ dependence of the subprocess cross sections are listed in Eq. (3.4);

Model	$\hat{\sigma}$(large $(\hat{s})^{1/2}$)
SM	$1/\hat{s}$
U	$1/\hat{s}$
l^*	$1/\Lambda^2$
$ZZ\gamma$	$\hat{s}^2/\Lambda^4 m_Z{}^2$
$Z\gamma\gamma$	$\hat{s}/\Lambda^4$
$ZJ\gamma$	$1/m_J{}^2$ (3.4)

Here appropriate angular and transverse-momentum cuts to avoid infrared divergences are understood. The $ZZ\gamma$ and $Z\gamma\gamma$ models have asymptotic behavior which must be modified by form factor or unitarity corrections at high $(\hat{s})^{1/2}$. The high-mass bump in the distribution of the $ZZ\gamma$ model should presumably be suppressed by a nonconstant form factor. The divergent behavior of the $Z\gamma\gamma$ model does not show up in its $(\hat{s})^{1/2}$ distribution since the convolution over the incident parton distributions drops faster than $1/\hat{s}$.

Figure 3(b) gives the $m(l^+l^-)$ distributions after all cuts. The data points are shown at the top of the figure with the error bars denoted by the horizontal lines. The peak at $m(l^+l^-)=m_U$ in the scalar-partner model is evident. In the excited-lepton model there is no *a priori* reason to expect m_{μ^*} to be equal to m_{e^*}.

Figure 4 shows the higher- and lower-$m(l\gamma)$ distributions. The lower-$m(l\gamma)$ distribution in Fig. 4(a) shows most strikingly the unlikelihood of all the anomalous models considered here. This distribution suggests that all alternative models provide unlikely explanations of the anomalous events.

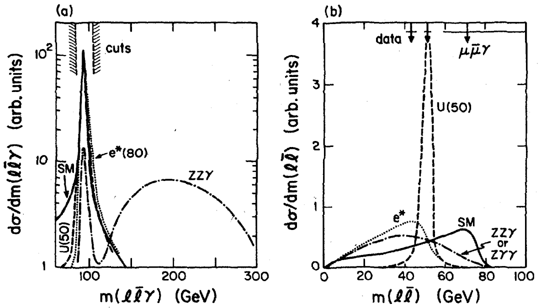

FIG. 3. Invariant-mass distributions in the process $p\bar{p}\to l^+l^-\gamma$ + anything, for the models of Figs. 1 and 2. (a) $m(l^+l^-\gamma)$, (b) $m(l^+l^-)$ with cuts described in the text.

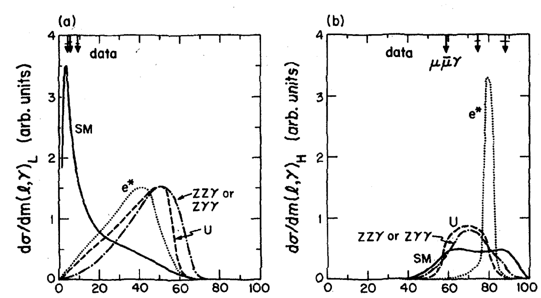

FIG. 4. Invariant-mass distributions with cuts: (a) lower-$m(l\gamma)$ and (b) higher-$m(l\gamma)$.

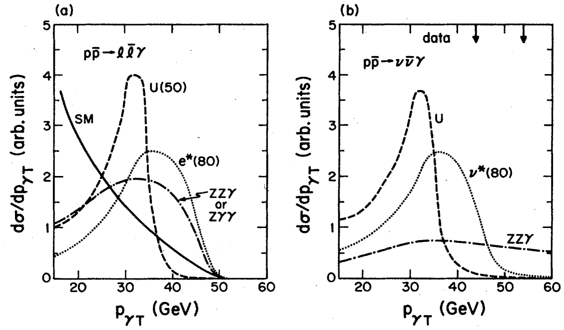

FIG. 5. Photon transverse-momentum distribution from the models of Figs. 1 and 2 for $Z\to l^+l^-\gamma$ decay. (a) $p\bar{p}\to l^+l^-\gamma+$ anything, (b) $p\bar{p}\to\nu\bar{\nu}\gamma+$ anything with cuts as described in the text.

C. Photon transverse-momentum distributions

Figure 5(a) shows the distributions in $p_{\gamma T}$, the photon momentum transverse to the beam axis. The published data have not quoted the $p_{\gamma T}$ values. The $p_{\gamma T}$ distribution is useful in studying rather model-independently whether the $l^+l^-\gamma$ events and the recently reported two "photon" $+$ missing p_T events[17] have a common origin. We note that there is a Jacobian peak at

$$p_{\gamma T}=\tfrac{1}{2}m_Z(1-m_U{}^2/m_Z{}^2)$$

in the distribution of the U-boson model.

The decays $Z\to\nu\bar{\nu}\gamma$ are naturally expected in some of the models considered here, with typical values of the ratio

$$R\equiv\frac{\Gamma(Z\to\nu\bar{\nu}\gamma)}{\Gamma(Z\to e^+e^-\gamma)}$$

as listed in Table I. In the scalar-partner model $Z\to\nu\bar{\nu}\gamma$ is expected provided that there exist light right-handed neutrinos. The ratio $R=3$ is obtained by assuming the universal $Uf\bar{f}$ coupling and three light ν_R's. In the excited-lepton model the ratio reads

$$R=3\frac{(f-f')^2(f+f'\tan^2\theta_W)^2}{(f+f')^2(f-f'\tan^2\theta_W)^2} \tag{3.5}$$

for three flavors provided that $m_{\nu^*}=m_{e^*}$. The R values for the $ZZ\gamma$ model and the $Z\gamma\gamma$ model are obtained from the standard Z and γ couplings to fermions. In the $ZJ\gamma$ model the R value is

$$R=3\frac{(a-b)^2}{(a+b)^2+4b^2} \tag{3.6}$$

for three flavors.

We show in Fig. 5(b) the $p_{\gamma T}$ distributions in the scalar-partner model, the excited-lepton model (assuming $m_{\nu^*}=80$ GeV), and the $ZZ\gamma$ model, without cuts on missing transverse momenta. Two UA1 data points[17] are also shown. The flat distribution of the $ZZ\gamma$ model is caused by the large $Z\gamma$-production cross section discussed previously and thus is not reliable. By introducing a strong form-factor suppression, we expect that the $ZZ\gamma$-model prediction becomes more similar to the corresponding distribution in Fig. 5(a).

The experimental signature of $Z\to\nu\bar{\nu}\gamma$ is an unbalanced single, high p_T photon. If the observed "γ" $+$ missing p_T events and the $Z\to e^+e^-\gamma$ events have a common origin, than their $p_{\gamma T}$ distributions should be similar.

TABLE I. Ratio $\Gamma(Z\to\nu\bar{\nu}\gamma)/\Gamma(Z\to e^+e^-\gamma)$ in various models.

Model	$\Gamma(Z\to\nu\bar{\nu}\gamma)/\Gamma(Z\to e^+e^-\gamma)$
U boson	3 (if light ν_R exist)
e^*	rather arbitrary (depends on $\nu_e^*,\nu_\mu^*,\nu_\tau^*$ masses and their couplings)
$ZZ\gamma$	5.9
$Z\gamma\gamma$	0
$ZJ\gamma$	0 to 6

IV. CONCLUSION

Dalitz plots for $l^+l^-\gamma$ final states provide a clean separation of alternative models for radiative Z-boson decays. The Dalitz-plot locations of the three observed events of this type have low probability in any of the proposed alternatives. Only bremsstrahlung in the standard model has reasonable agreement with the predicted distributions, although in this case the predicted event rate is too small. Higher-statistics data from future collider runs should easily resolve the issue.

Note added in proof. After submitting this paper, we learned of other suggested models in which $l^+l^-\gamma$ comes from sources, with mass near m_Z, other than the Z boson. See, e.g., M. Veltman, Phys. Lett. **139B**, 307 (1984); W. Haymaker and T. Matsuki, Louisiana State University report, 1984 (unpublished); B. Holdom, Stanford University Report No. ITP-765, 1984 (unpublished); W. J. Marciano, BNL Report No. BNL-34728, 1984 (unpublished); M. Matsuda and T. Matsuoka, Nagoya University Report No. DPNU-84-14, 1984 (unpublished). We thank M. Veltman for comments.

ACKNOWLEDGMENTS

We thank C. Goebel, F. Herzog, K. Hikasa, and C. S. Lim for discussions. This research was supported in part by the University of Wisconsin Research Committee with funds granted by the Wisconsin Alumni Research Foundation, and in part by the Department of Energy under Contract No. DE-AC02-76ER00881.

[1]G. Arnison *et al.* (UA1 Collaboration), Phys. Lett. **122B**, 103 (1983); **129B**, 273 (1982); M. Banner *et al.* (UA2 Collaboration), *ibid.* **122B**, 476 (1983).

[2]G. Arnison *et al.* (UA1 Collaboration), Phys. Lett. **126B**, 298 (1983); P. Bagnaia *et al.* (UA2 Collaboration), *ibid.* **129B**, 130 (1983).

[3]S. L. Glashow, Nucl. Phys. **22**, 579 (1961); S. Weinberg, Phys. Rev. Lett. **19**, 1264 (1967); A. Salam, in *Elementary Particle Theory: Relativistic Groups and Analyticity (Nobel Symposium No. 8),* edited by N. Svartholm (Almqvist and Wiksell, Stockholm, 1968), p. 367.

[4]The UA1 group also reports a $Z\rightarrow\mu^+\mu^-\gamma$ candidate and four $Z\rightarrow\mu^+\mu^-$ candidates: C. Rubbia, at Workshop on Proton Antiproton Collider Physics, Bern, 1984 (unpublished); J. Rohlf, at Physics of 21st Century Conference, Tucson, 1983 (unpublished).

[5]See, e.g., D. Albert, W. J. Marciano, D. Wyler, and Z. Parsa, Nucl. Phys. **B166**, 460 (1980).

[6]U. Baer, H. Fritzsch, and H. Faissner, Phys. Lett. **135B**, 313 (1984); R. D. Peccei, *ibid.* **136B**, 121 (1984); see also F. M. Renard, *ibid.* **116B**, 269 (1982); **126B**, 59 (1983).

[7]K. Enquist and J. Maalampi, Phys. Lett. **135B**, 329 (1984); N. Cabibbo, L. Maiani, and Y. Srivastava, *ibid.* **139B**, 459 (1984).

[8]G. Gounaris, R. Kögerler, and D. Schildknecht, Phys. Lett. **137B**, 261 (1984); see also F. M. Renard, Nucl. Phys. **B196**, 93 (1982).

[9]Y. Tomozawa, Phys. Lett. **139B**, 455 (1984); see also Renard (Ref. 8).

[10]M. J. Duncan and M. Veltman, Phys. Lett. **139B**, 310 (1984).

[11]D. W. Duke and J. F. Owens, Phys. Rev. D **30**, 49 (1984).

[12]F. A. Berends, R. Kleiss, and S. Jadach, Nucl. Phys. **B202**, 63 (1982).

[13]G. Sterman and S. Weinberg, Phys. Rev. Lett. **39**, 1436 (1977).

[14]A model with an unconventional Higgs scalar gives similar final-state distributions. See J. Lindfors, S.-Y. Chu, and B. R. Desai, University of California-Riverside Report No. UCR-TH-84-1 (unpublished).

[15]The terms proportional to $\partial_\mu Z^\mu$ vanish when we neglect fermion masses which couple to Z. In this limit, the three $ZZ\gamma$ couplings shown in Ref. 8 reduce to the two terms in (2.15) by the substitutions $(2G_1+G_2)/M_Z{}^2\rightarrow 2f_1/\Lambda^2$ and $G_3/M_Z{}^2 \rightarrow -2f_2/\Lambda^2$. We thank K. Hikasa for clarifying this point.

[16]C. N. Yang, Phys. Rev. **77**, 242 (1950).

[17]G. Arnison *et al.* (UA1 Collaboration), Phys. Lett. **139B**, 115 (1984).